Modeling of the Optical Properties of Cofacial Chromophore Pairs: Stilbenophane

Johannes Gierschner,*,† Hans-Georg Mack,† Dieter Oelkrug,† Isabella Waldner,‡ and Hermann Rau‡

Institute of Physical and Theoretical Chemistry, University of Tübingen, Auf der Morgenstelle 8, 72076 Tübingen, Germany, and FG Physical Chemistry, Institute of Chemistry, University of Hohenheim, 70593 Stuttgart, Germany

Received: October 2, 2003

Using electronic absorption and fluorescence spectroscopic techniques, as well as quantum chemical calculations, we have studied the electronic spectra of thia-bridged stilbenophane (TSP) with close cofacial contact of two *trans*-stilbene (*t*-SB) units. Compared to the *t*-SB monomer, the experimental consequences of the cofacial arrangement are (i) a splitting of the main absorption band with a weakly allowed emitting state, and (ii) a strongly red-shifted, unstructured emission spectrum with long fluorescence decay times. According to the theoretical investigations, the two *t*-SB units are strongly bent in the electronic ground state (S_0), because of repulsive $\pi-\pi$ overlap. In the first excited state (S_1), the *t*-SB units become almost planar, because of attractive $\pi^*-\pi^*$ overlap. As a consequence, the symmetry-forbidden $S_0 \leftrightarrow S_1$ transition couples strongly to interchromophore breathing modes of low frequency ($\nu_1 = 67$ cm^{-1}, $\nu_2 = 117$ cm^{-1}), yielding structureless spectra with large Stokes shifts. The features of the calculated spectra are in good agreement with the experimental data. The results indicate that strong intermolecular vibronic coupling is also responsible for "excimer-like" emission in organic molecular crystals of cofacially arranged molecules. Furthermore, the different geometries in the S_0 and S_1 states of TSP give evidence for the mechanism of [2+2]photodimerization of *t*-SB in solutions.

Introduction

The prediction of solid-state optical and photophysical properties of poly-π-conjugated organic molecules such as oligophenylenevinylenes (OPVs), oligophenylenes (OPs), and oligothiophenes (OTs) is of crucial importance for the molecular engineering of optoelectronic devices. However, theoretical modeling still suffers from a lack of a quantitative understanding of intermediate electronic coupling effects. The strength of intermolecular interactions is sensitively dependent on the mutual geometrical arrangement of adjacent molecules in the condensed phase. In single crystals, vacuum-grown thin films, and nano-aggregates of unsubstituted OPVs,[1−3] OPs,[4] and OTs,[5] the molecules are oriented with their long axes parallel to each other, but their short axes are arranged in a "T-shaped" manner (a "herringbone" arrangement). In these systems, the emission spectra are well-structured and similar to the spectra in solution,[3,6] thus indicating that the intermolecular vibronic coupling in T-shaped arrangements is weak. Only in the spectral region of the electronic origin is the intensity strongly reduced, compared to the solution spectra.[1] According to the theoretical treatment of Spano,[7] this decrease is due to the impact of electronic coupling between the molecules, resulting in a (partially) forbidden 0−0 transition.

For cofacial molecular arrangements, strong changes of the spectral features, compared to the isolated molecules, are observed. This type of arrangement is found in oligoacene single crystals such as pyrene[8] and perylene,[9] but also in several crystalline OPVs with electron-withdrawing substituents.[10−13] Moreover, cofacial dimers are assigned as being the responsible species for trap emission in many solid OPV[14] and polyphenylenevinylene[15] films. The typical spectral feature of the cofacial arrangement is an "excimer-like" emission, which displays a broad, unstructured fluorescence band that is strongly red-shifted against absorption. In addition, the fluorescence decay time increases by a factor of ∼100 against the single-molecule decay.[10−12,14,16]

Classical bimolecular excimers are characterized by a nonbonding electronic ground state (S_0) and a bonding excited state (S_1).[16] The repulsive interaction between the chromophores in the S_0 state result in an unstructured red-shifted emission band.[16,17] On the other hand, the absorption spectrum in solution resembles the vibrationally structured monomer spectrum, because of the large intermolecular separation in S_0. This large separation is not observed in ground-state dimers and molecular crystals of cofacially oriented molecules.[8] The influence of intermolecular separation on the fluorescence and absorption spectra can be well-studied in [*n*,*n*]paracyclophanes,[18] where the distance between the benzene rings is controlled by the length *n* of the $(CH_2)_n$ bridges. Paracyclophanes with $n > 4$ do not show excimer emission. The fluorescence and absorption spectra are vibrationally structured and resemble those of *para*-xylene. For $n = 4$, classical excimer behavior with unstructured fluorescence but structured absorption is observed, whereas for $n = 2$ and 3, both the fluorescence and absorption spectra become unstructured.[19] According to X-ray diffraction studies,[20,21] the benzene rings of [2,2]paracyclophane are strongly bent. This molecular structure was confirmed by quantum chemical calculations,[22,23] which also predict a significant decrease of the inter-ring separation in the first excited S_1 state.[23]

* Author to whom correspondence should be addressed. E-mail: johannes.gierschner@ipc.uni-tuebingen.de.
† University of Tübingen.
‡ University of Hohenheim.

10.1021/jp036952j CCC: $27.50
Published on Web 12/12/2003

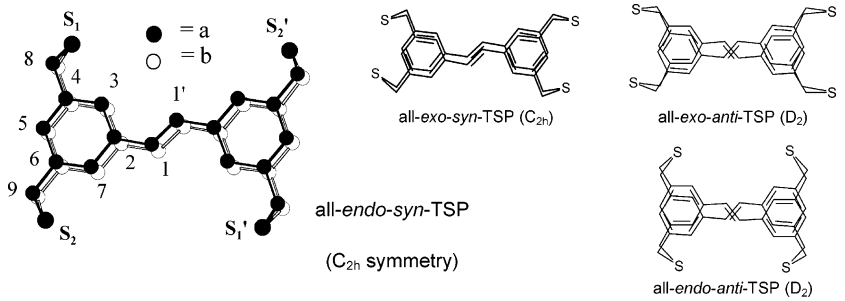

Figure 1. Structures of selected conformations of tetrathia-stilbenophane (TSP) and labeling of the atoms.

In three-dimensional molecular assemblies, nearest-neighbor interactions dominate the total interaction energy, because of the strong distance dependence of intermolecular electronic coupling. Thus, covalently linked dimers with a defined mutual arrangement of the chromophores can serve as model compounds for the investigation of intermolecular interactions in organic molecular crystals. Stilbenoid dimers with partial $\pi-\pi$ overlap of the chromophores, covalently linked by a paracyclophane core, were synthesized by Müllen[24] and Bazan,[25] and the electronic spectra of the dimers were investigated extensively, both experimentally and theoretically.[25,26] Stilbenophane with two $-CH_2-CH_2-$ bridges in the para positions was synthesized and characterized by Wennerström.[27] Stilbenoid dimers were also prepared by Lewis and Letsinger, using 1:1 mixtures of complimentary oligonucleotides that contained *trans*-stilbene (*t*-SB) units.[28]

In this contribution, we present a combined experimental and theoretical study on the optical and photophysical properties of a new model compound, tetrathia-stilbenophane (TSP)[29] (see Figure 1), with perfect cofacial arrangement of the *t*-SB units. The theoretical approach includes (i) the calculation of the electronic transition energies by semiempirical and ab initio quantum chemical methods and (ii) the calculation of the emission spectrum by a Franck−Condon analysis, based on ab initio and density functional theory (DFT) quantum chemical calculations, including the equilibrium geometries, vibrational frequencies, and nuclear displacements of the totally symmetric vibrational modes in the involved electronic states. For monomers, this approach was demonstrated to be very successful.[11,30,31] We expect, for this reason, that the method can also be expanded to dimers.

Experimental Section

Materials and Measurements. The synthesis, purification, and characterization of TSP were described elsewhere.[29] *t*-SB was purchased from Merck and used without further purification. The substances were dissolved in dioxane, and the fluorescence emission and excitation spectra were measured on a Spex model Fluorolog 222 spectrofluorimeter in a right-angle geometry.

Computational Details. The quantum chemical calculations, including (i) the adiabatic transition energies, (ii) the equilibrium geometries in the electronic ground state (S_0) and the first excited state (S_1), and (iii) the nuclear displacements of the vibrational modes, were performed at the ab initio Hartree−Fock (HF) and restricted configuration singles (RCIS) level of theory. The vibrational frequencies were obtained by a density functional approach (B3LYP), because the HF calculations are known to overestimate the experimental values by 5%−10%. All ab initio and DFT calculations were performed with the Gaussian 98 program system,[32] using the standard 6-311G* basis set. Vertical transition energies ($S_0 \rightarrow S_i$) of TSP were obtained by the semiempirical Zerner's spectroscopic parametrization for intermediate neglect of differential overlap (ZINDO/S) method,[33] coupled with a single configuration interaction (SCI) technique, which involved eight occupied and unoccupied molecular levels, corresponding to the first branches of π- and π*-type molecular orbitals. Hereby, the geometry was optimized with the AM1 (Austin Model 1) method.[34] All semiempirical AM1, PM3 (Parametric Method 3),[35] and ZINDO/S calculations were conducted with the HYPERCHEM program.[36]

The Franck−Condon calculations of the spectra were performed within the harmonic approximation of undistorted oscillators, including the progressions and combinational bands of the complete set of totally symmetric vibrational modes (details of the calculation are given in ref 30). The Franck−Condon factors, i.e., the squared overlap integrals between the vibrational quanta $p = 0$ in the initial electronic state *i* and the *q*th quanta of the final state (*f*) of each mode *k*, are given by

$$F_{q0}^2(k) = \frac{(S_k)^{q_k} e^{-S_k}}{q_k!} \tag{1}$$

where the Huang−Rhys factor (S_k) of each mode is calculated by

$$S_k = \left(\frac{2\pi^2 c}{h}\right)\nu_k(\Delta Q_k)^2 \tag{2}$$

where *h* is Planck's constant, *c* the velocity of light, ν_k the frequency of mode *k*, and ΔQ_k the projection of the geometry change between the two states (*i*, *f*). ΔQ_k can be calculated by[37]

$$\Delta Q_k = [\boldsymbol{x_f} - \boldsymbol{x_i}]\boldsymbol{M}^{1/2}\boldsymbol{L_{k,f}} \tag{3}$$

where $\boldsymbol{x_i}$ and $\boldsymbol{x_f}$ are the 3*N*-dimensional vectors of the equilibrium Cartesian coordinates in *i* and *f*, and $\boldsymbol{M}$ is the $3N \times 3N$ diagonal matrix of the atomic masses. $\boldsymbol{L_{k,f}}$ is the 3*N* vector of the normal coordinates of the vibrational mode. The Franck−Condon calculations of the spectra were performed with in-house programs.

For TSP, 17 different conformations are conceivable (Table 1), which are obtained by combinations of (i) the relative orientation of the two *t*-SB units (syn = parallel units, anti = crossed units) and (ii) the positions of the four sulfur atoms (endo/exo) (see Figure 1). According to the quantum chemical results, the most-stable conformations are those with all S atoms at the endo-positions (see Table 1). The energy differences between syn and anti configurations are very small or even negligible. Therefore, all geometry optimizations, calculations of electronic transition energies, molecular orbitals, and vibra-

TABLE 1: Relative Energies of the Different Conformations of Tetrathia-stilbenophane (TSP), as Obtained by the AM1 and PM3 Levels[a]

position of the sulfur atom[c]				*syn*-TSP					*anti*-TSP				
				point	relative energy (kcal/mol)				point	relative energy[b] (kcal/mol)			
S_1	S_2	S_1'	S_2'	group	AM1	PM3	HF	B3LYP	group	AM1	PM3	HF	B3LYP
endo	endo	endo	endo	C_{2h}	0.62	−0.16	0.61	0.17	D_2	0.00	0.00	0.00	0.00
exo	endo	endo	endo	C_s	0.97	0.37			C_1	0.50	0.62		
endo	exo	endo	endo	C_s	1.05	0.45							
exo	endo	exo	endo	C_{2h}	1.31	0.85			C_2	0.88	1.13		
endo	exo	endo	exo	C_{2h}	1.46	1.00							
endo	exo	exo	endo	C_s	1.54	1.17			C_2	1.00	1.26		
endo	endo	exo	exo	C_s	1.95	1.60			C_2	1.46	1.82		
exo	endo	exo	exo	C_s	2.44	2.24			C_1	2.07	2.47		
endo	exo	exo	exo	C_s	2.51	2.33							
exo	exo	exo	exo	C_{2h}	3.60	3.63	4.48	3.82	D_2	3.42	2.47	4.10	3.77

[a] Selected conformations were also calculated with the HF/6-311G* and B3LYP/6-311G* method. [b] The energy of the all-endo-*anti*-TSP conformation was set to zero. [c] For numbering of the sulfur atoms, see Figure 1.

TABLE 2: Electronic Transition Energies of *t*-SB and All-endo-*syn*-TSP

RCIS/6-311G* calculated, ν_{00} in vacuo (× 1000 cm^{-1})[a]		ZINDO/S calc.[b] ν_{vert} (× 1000 cm^{-1})	CI description	experimental band maxima in dioxane (× 1000 cm^{-1})
t-SB				
31.7 (1.219)		33.8 (1.267)	H → L	33.6
TSP				
29.2 (0.000)	$1B_g$	27.6 (0.000)	H → L	A_I 28.8
	$2B_g$	31.8 (0.000)	H → L + 2 (0.41) H - 2 → L (−0.40)	
	$1A_u$	31.9 (0.000)	H → L + 3 (0.41) H - 3 → L (−0.40)	
37.1 (1.985)	$1B_u$	32.5 (2.017)	H → L + 1	A_{II} 32.5
	$2B_u$	33.0 (0.043)	H → L + 5 (−0.36) H - 2 → L + 1 (0.34)	
	$2A_g$	33.0 (0.000)	H → L + 6 (0.36) H - 3 → L + 1 (0.34)	
	$3B_u$	36.0 (0.434)	H - 1 → L	A_{III} 35.8
	$3B_g$	37.6 (0.000)	H - 1 → L + 1	

[a] Adiabatic transmission energies (ν_{00}, theoretical oscillator strengths are given in parentheses). [b] Vertical transition energies (ν_{vert}) and CI description (main CI expansion coefficients of the configurations are given in parentheses), obtained at the semi-empirical ZINDO/S level.[39]

tional modes were performed for the highly symmetrical all-endo-*syn*-conformation (see Figure 1).

Experimental Results

The fluorescence emission and excitation spectra of TSP in dioxane are presented in Figure 2. The corresponding *t*-SB spectra are shown for comparison. At the low-energy side of the TSP absorption spectrum, an unstructured weak band (A_I) is observed at $\nu_{max} = 28\,800$ cm^{-1}, which is shifted by $\Delta\nu = -4700$ cm^{-1} to the red against the absorption maximum of *t*-SB. The main absorption band A_{II} is located at $\nu_{max} = 32\,500$ cm^{-1}, followed by a pronounced shoulder A_{III} at $\nu_{max} = 35\,800$ cm^{-1} (Table 2). TSP displays an unstructured excimer-like emission spectrum that is strongly red-shifted by $\Delta\nu_R \approx -7400$ cm^{-1} against the *t*-SB emission spectrum. In a first approximation, the fluorescence spectrum and the A_I band are mirror-symmetrical to each other (see Figure 2), with a mirror center at $\nu = 25\,000$ cm^{-1} that is assigned to the adiabatic transition energy $S_0 \leftrightarrow S_1$. The fluorescence quantum yield of TSP is low ($\Phi_F = 0.05$), and the fluorescence decay time was determined to $\tau_F = 11$ ns.[29] Thus, the natural lifetime of $\tau_F^0 = 220$ ns is larger than that of *t*-SB, by 2 orders of magnitude.[38]

The solid-state fluorescence emission and excitation spectra of TSP are only moderately changed, as compared to the spectra in dilute solution (see Figure 2). The relative intensities of the A_I and A_{II} bands in the fluorescence excitation spectrum differ from the solution spectra, because of the high optical density of the solid-state sample. The red-shift of the fluorescence spectrum by −1800 cm^{-1} against the solution spectrum of TSP

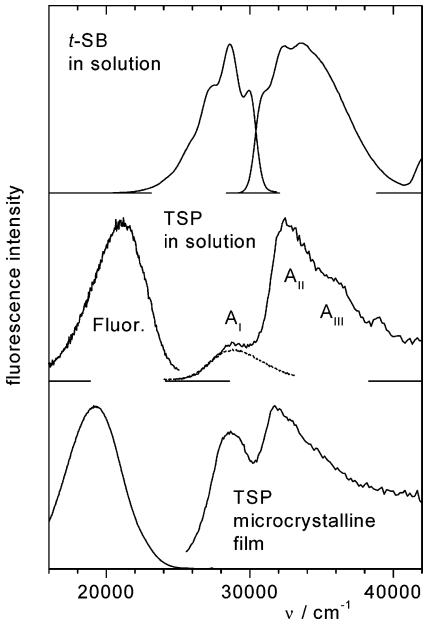

Figure 2. Fluorescence emission (left) and excitation (right) spectra of *t*-SB and TSP: (top) *t*-SB in dioxane; (center) TSP in dioxane (dashed line represents the fluorescence spectrum of TSP, mirrored at $\nu = 25\,000$ cm^{-1}); and (bottom) TSP microcrystalline film.

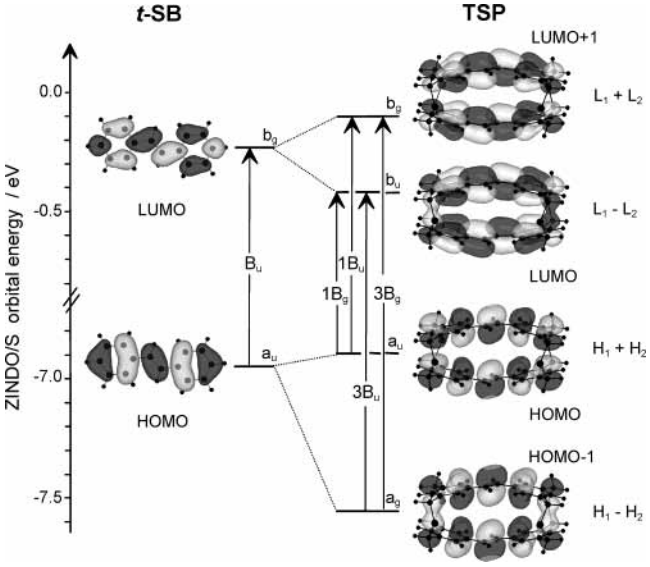

Figure 3. Correlation diagram of one-electron frontier molecular orbitals (MOs) of *t*-SB (left) and TSP (right), according to ZINDO/S calculations.

TABLE 3: Bond Lengths and Angles of All-endo-*syn*-TSP (C_{2h} Symmetry) in the Electronic Ground State S_0 and the Excited States $1B_g$ and $1B_u$, as Obtained by the HF/6-311G* and RCIS/6-311G* Approximation

atoms involved[b]	TSP			*t*-SB[a]	
	S_0 (A_g)	$1B_g$	$1B_u$	S_0 (A_g)	S_1 (B_u)
	Bond Lengths (Å)				
1-1′	1.326	1.369	1.363	1.327	1.409
1−2	1.478	1.433	1.443	1.477	1.406
2−3	1.394	1.412	1.410	1.396	1.430
	Angles (degrees)				
1′−1−2	126.9	126.5	126.0	127.1	125.4
1−2−3	123.3	123.6	123.2	123.7	123.4
	Interstilbene Distances (Å)				
1a−1b	4.346	3.788	4.474		
2a−2b	4.120	3.685	4.204		
3a−3b	3.878	3.533	3.934		
4a−4b	3.389	3.230	3.403		
5a−5b	3.204	3.099	3.211		
6a−6b	3.385	3.236	3.409		
7a−7b	3.877	3.547	3.944		

[a] The geometry of *t*-SB (C_{2h} symmetry) in the S_0 and S_1 states are shown for comparison. [b] For atom numbering, see Figure 1.

is mainly ascribed to the high polarizability of the solid material. The moderate changes of the spectral positions as compared to the solution spectra of TSP confirm the dominant contribution of nearest-neighbor interactions to the solid-state properties.

Discussion

Molecular Orbitals. The molecular orbitals (MOs) of all-endo-*syn*-TSP (see Figure 1) were calculated by the semiempirical ZINDO/S method after geometry optimization at the AM1 level. According to the correlation diagram between *t*-SB and TSP (Figure 3),[40] the frontier one-electron MOs of TSP are generated from the highest occupied molecular orbital (HOMO) (H_1, H_2) and lowest unoccupied molecular orbital (LUMO) (L_1, L_2) of the two *t*-SB units. The new HOMO (H) of the dimer is formed from the linear combination ($H_1 + H_2$) that is anti-bonding, with respect to the $\pi-\pi$ overlap between the two *t*-SB units. The new lower energetic H−1 orbital is formed from ($H_1 - H_2$) that is $\pi-\pi$ bonding. Accordingly, the new LUMO (L) is formed from ($L_1 - L_2$) that is $\pi^*-\pi^*$ bonding, and the new L + 1 from ($L_1 + L_2$) that is $\pi^*-\pi^*$ anti-bonding. The LCAO coefficients of the MOs in TSP are symmetrically delocalized over the two *t*-SB units (see Figure 3).[40] The energy gap $\Delta E_{H-1,H}$ is significantly larger than $\Delta E_{L,L+1}$, indicating a stronger interaction of the H_1, H_2 levels compared to the L_1, L_2 levels of the *t*-SB units. These results give clear evidence for strong electronic coupling of the *t*-SB units in TSP due to the small interchromophore separation *d* (Table 3). The influence of *d* on the energetic positions and LCAO coefficients of two cofacially oriented *t*-SB units were theoretically treated by Cornil et al. at the ZINDO/S level.[41] In the weak coupling regime ($d > 8$ Å), the splittings of H − 1 and H, and of L and L + 1, are negligible, the LCAO coefficients of a given orbital are localized on a single chain, and the electronic interactions between the *t*-SB units are sufficiently described by Kasha's molecular exciton model.[42] In the medium coupling regime (4 Å $< d <$ 8 Å), the LCAO coefficients of the MOs are delocalized over the two *t*-SB units, the degeneracy of the frontier MOs is revoked, and a symmetrical splitting of $\Delta E_{H-1,H} \approx \Delta E_{L,L+1}$ is found.[41] For strong electronic coupling ($d < 4$ Å), the splitting becomes $\Delta E_{H-1,H} > \Delta E_{L,L+1}$, in agreement with our results for TSP (see Figure 3), thus indicating that the electronic properties of TSP can be well understood by strong electronic interactions of the individual *t*-SB units.

Electronic Transition Energies. In a semiempirical quantum chemical approach, the vertical electronic transition energies were obtained at the semiempirical ZINDO/S level. This approximation is known to yield reasonable results for single OPV chains in solution.[43] According to the ZINDO/S calculations, the symmetry-forbidden lowest singlet transition ($1B_g$) of TSP, predicted at 27 500 cm^{-1}, is described by the H → L excitation and corresponds to the weak A_I band (see Table 2). The transition must borrow intensity by Herzberg−Teller coupling from the allowed A_{II} band via a_u vibrational modes. The low oscillator strength of the emitting $1B_g$ state is responsible for the low radiative rate constant of TSP. The second and third excited states ($2B_g$, $1A_u$) both are forbidden and involve MOs (L + *m*, H − *m*, with $m = 2, 3$) with LCAO coefficients located mainly at the phenyl moieties of the two *t*-SB units. According to our calculations, the intense A_{II} band of the experimental spectrum consists of two allowed transitions of B_u symmetry. The $1B_u$ state, located at 32 500 cm^{-1}, is described by the H → L + 1 excitation and mainly contributes to the high oscillator strength of the A_{II} band (see Table 2). The $2B_u$ state, which exhibits only a small oscillator strength, is located 500 cm^{-1} above $1B_u$. The H − 1 → L excitation results in the $3B_u$ transition, located at 36 000 cm^{-1}. According to the spectral position and oscillator strength of $3B_u$ (see Table 2), the transition corresponds to the A_{III} band of the experimental spectrum, whereas the assignment of A_{III} as a vibronic progression of the A_{II} band is unlikely, because of the large energy separation of $\Delta\nu(A_{III} - A_{II}) = 3300$ cm^{-1}. The diversity of electronic transitions in the ZINDO/S calculation results from the strong electronic interaction between the *t*-SB units in TSP. Thus, the description within Kasha's molecular exciton model is a too-simplified approximation for the cofacial "H-aggregate" of two *t*-SB units.

The adiabatic transition energies of TSP were obtained at the ab initio RCIS/6-311G* level. For *t*-SB, the calculated transition energy yields $\nu_{00} = 31\,700$ cm^{-1}, which is in excellent agreement with the experimental value in vacuo ($\nu_{00} = 31\,500$ cm^{-1}).[30] For TSP, the RCIS calculations only reproduce the A_I

and A_{II} bands of the experimental spectrum (see Table 2). The lower symmetry-forbidden singlet transition is described by a predominant contribution of the H → L excitation, analogous to the ZINDO/S results. In contrast to the ZINDO/S calculations, the A_{II} band is predicted at the RCIS level to be a mixture of H → L + 1 and H − 1 → L excitations with approximately equal weights. This could indicate that the interaction strength between the *t*-SB units is weaker, compared to the ZINDO/S calculation, maybe due to the fact that, at the RCIS level of theory, electron correlation effects are insufficiently taken into consideration. Also, the $1B_u$ adiabatic transition energy, calculated at the RCIS level to $\nu_{00}(1B_u) = 37\,100$ cm^{-1} (see Table 2), is in rather poor agreement with the experiment, and the $1B_g$ adiabatic transition energy at $\nu_{00}(1B_g) = 29\,200$ cm^{-1} is also considerably higher than the experimental $S_0 \leftrightarrow S_1$ electronic origin. However, one must recall that solvent effects were neglected in the RCIS calculations, which results in a significant blue shift against the experimental spectrum of ∼2000 cm^{-1}.[30]

Geometrical Structure. The short $-CH_2-S-CH_2-$ bridges force the two *t*-SB units of TSP into a close cofacial arrangement. According to HF/6-311G* calculations, the *t*-SB units are strongly bent, to minimize the repulsive interaction in the S_0 state. Hence, the interstilbene distances (see Figure 1) vary from d(1a−1b) = 4.35 Å to d(5a−5b) = 3.20 Å (see Table 3). The repulsive interaction between the *t*-SB units in the S_0 state results from the anti-bonding $\pi-\pi$ overlap between the two *t*-SB units in the HOMO orbital of TSP (see Figure 3), similar to the situation in [2,2]paracyclophane.[44] The intrastilbene $C_1-C_{1'}$ and C_1-C_2 bond lengths, as well as the $C_{1'}-C_1-C_2$ bond angle, are almost identical to those in *t*-SB, displaying the same pronounced bond alternation in the vinylene moiety as that in the monomer (see Table 3).

In the S_1 ($1B_g$) state of TSP, the interstilbene separation between the two vinylene units a and b is strongly reduced against S_0 by $\Delta x \approx -0.5$ Å (see Table 3). The *t*-SB units are now almost planar. The decrease of the interstilbene separation upon $S_0 \rightarrow S_1$ electronic excitation is due to the promotion of an electron from the HOMO level to the LUMO level. The latter is characterized by the bonding $\pi^*-\pi^*$ overlap between the *t*-SB units (see Figure 3). In addition, the $C_1-C_{1'}$ bonds are lengthened and the C_1-C_2 bonds are shortened, as compared to the S_0 state. The relative changes in the bond lengths (Δr) are equal to approximately one-half of the values in *t*-SB (see Table 3), because the two *t*-SB units are excited simultaneously upon promotion of the electron to the LUMO level.

Vibrational Fine Structure of the Electronic Spectra. The nuclear geometries of the S_0 and S_1 states were used to derive the vibrational fine structure of the electronic transitions. According to eqs 1−3, the vibrational structure of the fluorescence and absorption spectra is dominated by modes, whose nuclear displacements essentially coincide with the geometrical changes after the electronic transition. The larger the coupling efficiency (the Huang−Rhys factor, S_k), the larger the Franck−Condon factors ($F^2_{q0}(k)$) for excitations to higher quantum numbers q of the final electronic state. For $S_k \ll 1$, the envelope of the progression becomes exponential, whereas for $S_k \gg 1$, the envelope is of Gaussian type, with the mean value of the distribution given by $\bar{\nu}_k = \nu_{00} - S_k\nu_k$, where ν_{00} is the adiabatic transition energy. Hence, the overall red shift of the emission spectrum is a sensitive function of the number of modes with large coupling efficiencies.

In *t*-SB, the geometrical changes upon $S_0 \rightarrow S_1$ electronic excitation are preliminarily due to changes in the bond lengths and angles of the vinylene moiety (see Table 3). Of the 25 vibrations of a_g symmetry in *t*-SB, which may serve as coupling modes to the electronic transition, only a few in-plane stretching modes efficiently couple and display moderate Franck−Condon activity, with Huang−Rhys factors of $S \leq 0.8$,[30] in good agreement with low-temperature measurements on *t*-SB.[30,45,46] The low-temperature spectra are well-structured and, in a first approximation, the absorption and fluorescence spectra are mirror-symmetrical to each other, because of similar nuclear displacements of the a_g modes in the S_0 and S_1 states.[30] At room temperature, the spectra are broadened because of (i) inhomogeneities of the environment and (ii) the excitation of phenyl−vinyl torsional modes (ν_{tors}). The fluorescence spectrum still is structured, whereas the absorption spectrum becomes unstructured and asymmetrically shifted to the blue (see Figure 2). The differences between the fluorescence and absorption spectra are caused by the steeper potential of ν_{tors} in the S_1 state, as compared to that in the S_0 state.[45] The calculated spectra (Figure 4), taking into account the complete set of a_g modes as well as the low-frequency torsional modes in the S_0 and S_1 states, which were determined in jet-cooled spectra of *t*-SB,[45] are in good agreement with the experimental spectra (see Figure 2). The blue shift of 1700 cm^{-1} of the calculated spectra, as compared to the experimental spectra, is entirely due to the neglect of solvent effects in the calculation.[30]

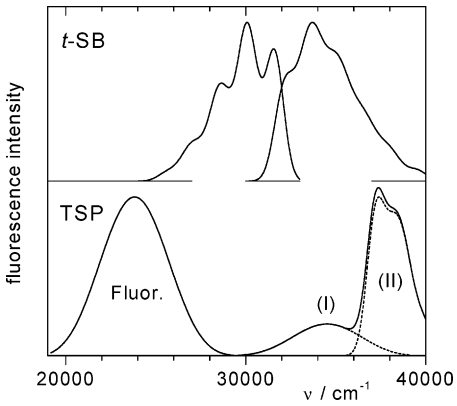

Figure 4. Fluorescence and absorption room-temperature spectra in vacuo, calculated at the ab initio HF/6-311G* and RCIS/6-311G* level, according to eqs 1−3, including the complete sets of a_g vibrational modes. Spectra were convoluted with a Gaussian distribution to account for inhomogeneous broadening (inserted Gaussian half-widths of γ = 1100 cm^{-1}); the top portion shows the spectra of *t*-SB. In addition, the thermal excitation of phenyl−vinyl torsional modes (ν_{tors}) was taken into consideration, with $\nu_{tors}(S_0) = 8$ cm^{-1}, $\nu_{tors}(S_1) = 48$ cm^{-1}; the bottom portion of the figure shows the spectra of TSP. The relative intensity of the A_I band was set to $0.2A_{II}$.

The geometrical changes in the bond lengths and angles of the vinylene moieties upon electronic excitation are, less pronounced, also observed for TSP. However, the *main* geometrical change is due to the decrease of the interstilbene separation (see Table 3). Therefore, a strong contribution of interstilbene breathing modes to the overall vibrational coupling is expected. Indeed, the most prominent mode in the fluorescence spectrum of TSP is a low-frequency pure interstilbene breathing mode calculated at $\nu_A = 67$ cm^{-1}, which displays extremely large Franck−Condon activity, with a Huang−Rhys factor of $S_A = 7.0$ (Figure 5). Thus, the envelope of this vibrational progression is approximately Gaussian-shaped. Also, the mode at $\nu_B = 117$ cm^{-1} ($S_B = 2.5$; see Figure 5), as well as several additional modes in the frequency range up to 1800 cm^{-1} with moderate Franck−Condon activities ($S \approx 1$) exhibit significant contributions of interstilbene motions. The efficiently

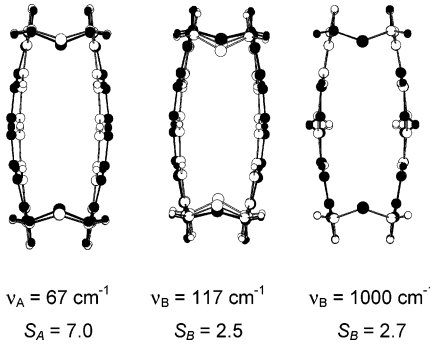

Figure 5. Vibrational displacements of the most prominent modes of TSP (side view); the two substructures, represented as open and solid symbols, give the relative displacements of the atoms in the ±-directions. The sum of the squared displacements of all atoms equals unity.

coupling mode at $\nu_C = 1000$ cm^{-1} ($S_C = 2.7$) is a localized breathing motion of the vinylene moieties, where the strongest contribution is given by the vinylene C−H deformation (see Figure 5). The emission spectrum was calculated including the progressions and combination bands of the complete set of a_g modes. Already at a temperature of $T \rightarrow 0$ K (i.e., without considering any spectral broadening), the calculated spectrum is poorly structured and the maximum is red-shifted by ca. −5000 cm^{-1} against the spectral origin. To account for inhomogeneous broadening at room temperature, the spectrum was additionally convoluted by a Gaussian distribution (half-width of $\gamma = 1100$ cm^{-1}, see Figure 4). The large Stokes shift and the envelope of the calculated spectrum is in good agreement with the experimental spectrum (see Figure 2).

The results emphasize that the emission properties of interacting chromophores are very sensitive to the intermolecular arrangement. In T-shaped arrangements, which are favored, for example, by stilbene homologous compounds in the condensed phase,[1−3] interchromophore vibrations have a minor role for electron−phonon coupling, and the spectra are similar to those of the isolated molecules.[1,6] In perfect cofacial arrangements of π-conjugated organic chromophores, the main geometrical change upon electronic excitation is the decrease of the interchromophore distance, as it was stated in the literature for pyrene excimers[8] and [2,2]paracyclophane.[23] The present study shows that this decrease leads to a strong coupling of interchromophore vibrations to the electronic transition. This type of coupling is responsible for the strongly red-shifted, unstructured "excimer-like" emission spectra.

Figure 4 furthermore presents the calculated $1A_g \rightarrow 1B_g$ (A_I) and $1A_g \rightarrow 1B_u$ (A_{II}) absorption spectra of TSP. The relative intensity of the symmetry-forbidden A_I band was adopted from the experimental spectrum to allow for Herzberg−Teller coupling to the A_{II} band. In contrast to the calculated A_I band, which is mirror-symmetrical to the emission spectrum, the A_{II} band is narrower and somewhat structured, in reasonable agreement with experiment. The different spectral features of the A_{II} band, compared to A_I, are due to the geometry of the $1B_u$ state, where the interstilbene separation is much larger than in the $1B_g$ state and resembles that of the S_0 ($1A_g$) state (see Table 3). Concomitantly, interstilbene breathing modes have a minor role in the overall coupling efficiency of the vibrational modes to the $1A_g \rightarrow 1B_u$ transition; e.g., for the breathing mode at $\nu_A = 67$ cm^{-1} (see Figure 5), the Huang−Rhys factor is now only $S_A = 0.5$.

Conclusions

Thia-bridged stilbenophane (TSP) was investigated as a model compound for cofacial molecular arrangements in organic molecular crystals that display "excimer-like" emission. The geometries in the electronic ground-state S_0 ($1A_g$) and excited states ($1B_g$, $1B_u$), as well as the oscillator strengths, spectral positions, and vibrational fine structures of the emission and absorption bands of TSP, were revealed by quantum chemical calculations.

The energetic positions and intensities of the electronic transitions can be well understood by strong electronic interactions of the cofacially oriented *trans*-stilbene (*t*-SB) units in TSP. The weak A_I band, strongly red-shifted against the main absorption band of *t*-SB, corresponds to the symmetry-forbidden $1B_g$ state. The $1B_g$ state gains some intensity by Herzberg−Teller coupling and is responsible for the low radiative rate constant of TSP. The lack of vibrational fine structure of the excimer-like emission spectrum of TSP is caused by strong vibronic coupling. Upon $S_0 \rightarrow S_1$ electronic excitation, the distance between the two *t*-SB units strongly decreases, because of promotion of an electron from the $\pi-\pi$ anti-bonding highest occupied molecular orbital (HOMO) to the $\pi^*-\pi^*$ bonding lowest unoccupied molecular orbital (LUMO). Therefore, interstilbene breathing modes couple efficiently to the electronic transition and display an extremely large Franck−Condon activity, which leads to the unstructured, Gaussian-shaped, and strongly Stokes-shifted emission spectrum. The $1A_g \rightarrow 1B_g$ absorption spectrum is mirror-symmetrical to the emission spectrum, whereas the $1A_g \rightarrow 1B_u$ absorption spectrum is narrow and structured, because of the $\pi^*-\pi^*$ anti-bonding character of the allowed $1B_u$ state. The results give evidence that the strong vibronic coupling of adjacent cofacially oriented molecules is also responsible for the excimer-like emission of cofacial molecular arrangements in organic molecular crystals.

The difference between the electronic interactions of the *t*-SB units in the S_0 and S_1 states of TSP has important implications, in regard to the photochemistry of *t*-SB monomers. The repulsive interaction of cofacial *t*-SB pairs in the electronic ground state predicts that ground-state dimers in solutions of *t*-SB are not stable, even at high concentrations. Upon irradiation, the attractive interaction of the *t*-SB units in the S_1 state leads to the diffusion-controlled formation of excimers, which is the first step for the [2+2]photodimerization of *t*-SB. Hence, cofacial stilbenoid dimers[28] and stilbenophanes[27,29] are thermally stable in the electronic ground state, where the interstilbene separation is too large to enable [2+2]cycloaddition, whereas this process becomes efficient upon irradiation with UV light.[27−29]

Acknowledgment. We thank S. Schweizer and B. Doser for recording the spectra of TSP, and the HRLS (Stuttgart, Germany) for access to substantial computer time. The authors also acknowledge financial support by the Fonds der Chemischen Industrie and by the European Union (through Grant No. HPRN-CT-2002-00323).

References and Notes

(1) Wu, C. C.; Korovyanko, O. J.; DeLong, M. C.; Vardeny, Z. V.; Ferraris, J. P. *Synth. Met.* **2003**, *139*, 735−738.

(2) van Hutten, P. F.; Wildemann, J.; Meetsma, A.; Hadziioannou, G. *J. Am. Chem. Soc.* **1999**, *121*, 5910−5918.

(3) Vaday, S.; Geiger, H. C.; Cleary, B.; Perlstein, J.; Whitten, D. G. *J. Phys. Chem. B* **1997**, *101*, 321−329.

(4) Baker, K. N.; Fratini, A. V.; Resch, T.; Knachel, H. C.; Adams, W. W.; Socci, E. P.; Farmer, B. L. *Polymer* **1993**, *34*, 1571−1587.

(5) (a) Antolini, L.; Horowitz, G.; Kouki, F.; Garnier, F. *Adv. Mater.* **1998**, *10*, 382−385. (b) Siegrist, T.; Kloc, C.; Laudise, R. A.; Katz, H. E.; Haddon, R. C. *Adv. Mater.* **1998**, *10*, 379−382.

(6) (a) Oelkrug, D.; Egelhaaf, H.-J.; Gierschner, J.; Tompert, A. *Synth. Met.* **1996**, *76*, 249−253. (b) Egelhaaf, H.-J.; Gierschner, J.; Oelkrug, D.

Synth. Met. **1996**, *83*, 221−226. (c) Gierschner, J.; Egelhaaf, H.-J.; Oelkrug, D. *Synth. Met.* **1997**, *84*, 529−530. (d) Oelkrug, D.; Tompert, A.; Gierschner, J.; Egelhaaf, H.-J.; Hanack, M.; Hohloch, M.; Steinhuber, E. *J. Phys. Chem. A* **1998**, *102*, 1902−1907.

(7) (a) Spano, F. C. *J. Chem. Phys.* **2001**, *114*, 5376−5390. (b) Spano, F. C. *J. Chem. Phys.* **2002**, *116*, 5877−5891. (c) Spano, F. C. *J. Chem. Phys.* **2002**, *117*, 9961. (d) Spano, F. C. *J. Chem. Phys.* **2003**, *118*, 981−994.

(8) (a) Camerman, A.; Trotter, J. *Acta Crystallogr.* **1965**, *18*, 636−643. (b) Hazell, A. C.; Larsen, F. K.; Lehmann, M. S. *Acta Crystallogr., Sect. B: Struct. Crystallogr. Cryst. Chem.* **1972**, *B28*, 2977−2984.

(9) Camerman, A.; Trotter, J. *Proc. R. Soc. London A* **1964**, *A279*, 129−146.

(10) Cohen, M. D.; Green, B. S.; Ludmer, Z.; Schmidt, G. M. J. *Chem. Phys. Lett.* **1970**, *7*, 486-490.

(11) Gierschner, J.; Egelhaaf, H.-J.; Mack, H.-G.; Oelkrug, D.; Martinez-Alvarez, R.; Hanack, M. *Synth. Met.* **2003**, *137*, 1449−1450.

(12) van Hutten, P. F.; Krasnikov, V. V.; Brouwer, H.-J.; Hadziioannou, G. *Chem. Phys.* **1999**, *241*, 139−154.

(13) Renak, M. L.; Bartholomew, G. P.; Wang, S.; Ricotto, P. J.; Lachicotte, R. J.; Bazan, G. C. *J. Am. Chem. Soc.* **1999**, *121*, 7787−7799.

(14) Schweikart, K.-H.; Hohloch, M.; Steinhuber, E.; Hanack, M.; Lüer, L.; Gierschner, J.; Egelhaaf, H.-J.; Oelkrug, D. *Synth. Met.* **2001**, *121*, 1641−1642.

(15) (a) Schaller, R. D.; Lee, F. L.; Johnson, J. C.; Haber, L. H.; Saykally, R. J.; Vieceli, J.; Benjamin, I.; Nguyen, T.-Q.; Schwartz, B. J. *J. Phys. Chem. B* **2002**, *106*, 9496−9506. (b) Bjorklund, T. G.; Lim, S.-H.; Bardeen, C. J. *J. Phys. Chem. B* **2001**, *105*, 11970−11977. (c) Whitelegg, S. A.; Buckley, A.; Rahn, M. D.; Fox, A. M.; Bradley, D. D. C.; Palsson, L. O.; Samuel, I. D. W.; Webster, G. R.; Burn, P. L. *Synth. Met.* **2001**, *119*, 575−576. (d) Jakubiak, R.; Yan, M.; Wan, W. C.; Hsieh, B. R.; Rothberg, L. J. *Isr. J. Chem.* **2000**, *40*, 153−157. (e) Huser, T.; Yan, M. *Synth. Met.* **2001**, *116*, 333−337. (f) Harrison, N. T.; Baigent, D. R.; Samuel, I. D. W.; Friend, R. H.; Grimsdale, A. C.; Moratti, S. C.; Holmes, A. B. *Phys. Rev.* **1996**, *B53*, 15815−15822.

(16) Förster, T.; Kasper, K. *Z. Elektrochem.* **1955**, *59*, 976−980.

(17) Stevens, B.; Ban, M. I. *Trans. Faraday Soc.* **1964**, *60*, 1515−1523.

(18) Cram, D. J.; Allinger, N. L.; Steinberg, H. *J. Am. Chem. Soc.* **1954**, *76*, 6132−6141.

(19) Vala, M. T., Jr.; Haebig, J.; Rice, S. A. *J. Chem. Phys.* **1965**, *43*, 886−897.

(20) Cram, D. J.; Steinberg, H. *J. Am. Chem. Soc.* **1951**, *73*, 5691−5704.

(21) Brown, C. J.; Farthing, A. C. *Nature* **1949**, *164*, 915−916.

(22) Henseler, D.; Hohlneicher, G. *J. Phys. Chem.* **1998**, *102*, 10828−10833.

(23) Canuto, S.; Zerner, M. C. *Chem. Phys. Lett.* **1989**, *157*, 353−358.

(24) Schenk, R.; Gregorius, H.; Meerholz, K.; Heinze, J.; Müllen, K. *J. Am. Chem. Soc.* **1991**, *113*, 2634−2647.

(25) Bazan, G. C.; Oldham, W. J., Jr.; Lachicotte, R. J.; Tretiak, S.; Chernyak, V.; Mukamel, S. *J. Am. Chem. Soc.* **1998**, *120*, 9188−9204.

(26) (a) Oldham, W. J., Jr.; Mio, Y.-J.; Lachicotte, R. J.; Bazan, G. C. *J. Am. Chem. Soc.* **1998**, *120*, 419−420. (b) Wang, S.; Bazan, G. C.; Tretiak, S.; Mukamel, S. *J. Am. Chem. Soc.* **2000**, *122*, 1289−1297. (c) Verdal, N.; Godbout, J. T.; Perkins, T. L.; Bartholomew, G. P.; Bazan, G. C.; Myers Kelley, A. *Chem. Phys. Lett.* **2000**, *320*, 95−103. (d) Moran, A. M.; Bartholomew, G. P.; Bazan, G. C.; Myers Kelley, A. *J. Phys. Chem. A* **2002**, *106*, 4928−4937. (e) Zyss, J.; Ledoux, I.; Volkov, S.; Chernyak, V.; Mukamel, S.; Bartholomew, G. P.; Bazan, G. C. *J. Am. Chem. Soc.* **2000**, *122*, 11956−11962. (f) Bartholomew, G. P.; Ledoux, I.; Mukamel, S.; Bazan, G. C.; Zyss, J. *J. Am. Chem. Soc.* **2003**, *124*, 13480−13485.

(27) Anger, I.; Sandros, K.; Sundahl, M.; Wennerström, O. *J. Phys. Chem.* **1993**, *97*, 1920−1923.

(28) (a) Letsinger, R. L.; Wu, T. *J. Am. Chem. Soc.* **1994**, *116*, 811−812. (b) Letsinger, R. L.; Wu, T. *J. Am. Chem. Soc.* **1995**, *117*, 7323−7328. (c) Lewis, F. D.; Wu, T.; Burch, E. L.; Bassani, D. M.; Yang, Y.-S.; Schneider, S.; Jäger, W.; Letsinger, R. L. *J. Am. Chem. Soc.* **1995**, *117*, 8785−8792.

(29) Rau; H.; Waldner, I. *Phys. Chem. Chem. Phys.* **2002**, *4*, 1776−1780.

(30) Gierschner, J.; Mack, H.-G.; Lüer, L.; Oelkrug, D. *J. Chem. Phys.* **2002**, *116*, 8596−8609.

(31) Gierschner, J.; Mack, H.-G.; Egelhaaf, H.-J.; Schweizer, S.; Doser, B.; Oelkrug, D. *Synth. Met.* **2003**, *138*, 311−315.

(32) Frisch, M. J.; Trucks, G. W.; Schlegel, H. B.; Scuseria, G. E.; Robb, M. A.; Cheeseman, J. R.; Zakrzewski, V. G.; Montgomery, J. A., Jr.; Stratmann, R. E.; Burant, J. C.; Dapprich, S.; Millam, J. M.; Daniels, A. D.; Kudin, K. N.; Strain, M. C.; Farkas, O.; Tomasi, J.; Barone, V.; Cossi, M.; Cammi, R.; Mennucci, B.; Pomelli, C.; Adamo, C.; Clifford, S.; Ochterski, J.; Petersson, G. A.; Ayala, P. Y.; Cui, Q.; Morokuma, K.; Malick, D. K.; Rabuck, A. D.; Raghavachari, K.; Foresman, J. B.; Cioslowski, J.; Ortiz, J. V.; Stefanov, B. B.; Liu, G.; Liashenko, A.; Piskorz, P.; Komaromi, I.; Gomperts, R.; Martin, R. L.; Fox, D. J.; Keith, T.; Al-Laham, M. A.; Peng, C. Y.; Nanayakkara, A.; Gonzalez, C.; Challacombe, M.; Gill, P. M. W.; Johnson, B. G.; Chen, W.; Wong, M. W.; Andres, J. L.; Head-Gordon, M.; Replogle, E. S.; Pople, J. A. *Gaussian 98*, revision A.7; Gaussian, Inc.: Pittsburgh, PA, 1998.

(33) Zerner, M. C. In *Reviews in Computational Chemistry*; Lipkowitz, K. B., Boyd, D. B., Eds.; VCH: New York, 1991; Vol. II, pp 313−365.

(34) Dewar, M. J. S.; Zoebish, E. G.; Healy, E. F.; Stewart, J. J. P. *J. Am. Chem. Soc.* **1985**, *107*, 3902−3909.

(35) Stewart, J. J. P. *J. Comput. Chem.* **1989**, *10*, 209−220.

(36) Hyperchem 6.0, Hypercube, Inc., Gainesville, FL, 1999.

(37) Negri, F.; Zgierski, M. Z. *J. Chem. Phys.* **1994**, *100*, 2571−2587.

(38) Mazzucato, U. *Pure Appl. Chem.* **1982**, *54*, 1705−1721.

(39) The more appropriate model monomer, stilbenetetramethanethiol, has not been synthesized yet. ZINDO/S calculations on this molecule reveal only small differences to *t*-SB, concerning the molecular orbitals as well as the electronic structure of the molecule. The electronic transition energy is calculated to be 1300 cm^{-1} lower, compared to that for *t*-SB (see Table 2), because of the inductive effect of the methanethiol groups.

(40) For higher (lower) orbitals, $L + m$ ($H - m$), with $m = 2-5$, the LCAO coefficients are mainly located at the phenyl moieties of the two *t*-SB units.

(41) Cornil, J.; dos Santos, D. A.; Crispin, X.; Silbey, R.; Brédas, J. L. *J. Am. Chem. Soc.* **1998**, *120*, 1289−1299.

(42) (a) Hochstrasser, R. M.; Kasha, M. *Photochem. Photobiol.* **1964**, *3*, 317−331. (b) Kasha, M.; Rawls, H. R.; El-Bayoumi, M. A. *Pure Appl. Chem.* **1965**, *11*, 371−392.

(43) Cornil, J.; Beljonne, D.; Brédas, J. L. *J. Chem. Phys.* **1995**, *103*, 834−841.

(44) Canuto, S.; Zerner, M. C. *J. Am. Chem. Soc.* **1990**, *112*, 2114−2120.

(45) Suzuki, T.; Mikami, N.; Ito, M. *J. Phys. Chem.* **1986**, *90*, 6431−6440.

(46) (a) Syage, J. A.; Felker, P. M.; Zewail, A. H. *J. Chem. Phys.* **1984**, *81*, 4685−4705. (b) Spangler, L. H.; van Zee, R.; Zwier, T. S. *J. Phys. Chem.* **1987**, *91*, 2782−2786. (c) Urano, T.; Hamaguchi, H.; Tasumi, M.; Yamanouchi, K.; Tsuchiya, S.; Gustafson, T. L. *J. Chem. Phys.* **1989**, *91*, 3884−3894. (d) Dyck, R. H.; McClure, D. S. *J. Chem. Phys.* **1962**, *36*, 2326−2345.